Probing reaction dynamics at metal surfaces with H_2 diffraction

2007 J. Phys.: Condens. Matter 19 305003

(http://iopscience.iop.org/0953-8984/19/30/305003)

J. Phys.: Condens. Matter **19** (2007) 305003 (18pp) doi:10.1088/0953-8984/19/30/305003

TOPICAL REVIEW

Probing reaction dynamics at metal surfaces with H_2 diffraction

D Farías[1], H F Busnengo[2] and F Martín[3]

[1] Departamento de Física de la Materia Condensada and Instituto Nicolás Cabrera, Universidad Autónoma de Madrid, Cantoblanco, 28049 Madrid, Spain
[2] Instituto de Física de Rosario and Universidad Nacional de Rosario, 2000 Rosario, Argentina
[3] Departamento de Química, Universidad Autónoma de Madrid, Cantoblanco, 28049 Madrid, Spain

E-mail: daniel.farias@uam.es, busnengo@ifir.edu.ar and fernando.martin@uam.es

Received 5 February 2007, in final form 20 April 2007
Published 13 July 2007
Online at stacks.iop.org/JPhysCM/19/305003

Abstract

We review recent experimental and theoretical work aimed to understand the reaction dynamics of hydrogen molecules at metal surfaces. Diffraction experiments and calculations using *ab initio* determined six-dimensional potential energy surfaces were carried out on several single-crystal surfaces: NiAl(110), Pt(111), Pd(111) and Pd(110). We discuss the general trends observed in the energy range studied (20–150 meV) when going from non-reactive to very reactive surfaces as well as specific features of the dynamics which can be seen in diffraction studies.

(Some figures in this article are in colour only in the electronic version)

Contents

1. Introduction

Owing to its importance in hydrogenation catalysis, the interaction of hydrogen with metal surfaces has been extensively studied in recent years, both experimentally [1, 2] and theoretically [3–6]. The design of better catalysts requires a detailed knowledge of the underlying reaction mechanism, in particular that leading to dissociation of H_2. Molecular beam and associative desorption experiments have been carried out to understand the main factors that govern H_2 dissociation at the surface [7–9]. In addition, vibrationally inelastic [10–14] and rotationally inelastic [15–17] scattering experiments have provided useful information on how certain features of the potential energy surface (PES) control the experimental observations. A usual limitation of these experiments is that they provide information averaged over the whole unit cell ([2] and references therein).

A different point of view is provided by diffraction experiments. As is well known, He-atom scattering (HAS) is a common tool to investigate surface properties [18]. In these experiments, the positions of the different diffraction peaks provide detailed information on the surface structure. Moreover, the relative intensities of the peaks are directly connected with the corrugation of the particle–surface PES. Thus, H_2 diffraction has been proposed some time ago as a promising (and maybe unique) experimental technique to measure the H_2–surface PES within the unit cell [19, 20]. However, these expectations have not yet been satisfied due to practical limitations in both theory and experiments.

The link between the experimental H_2 diffraction spectra and the PES can only be established by performing accurate dynamical calculations. In general, H_2 diffraction intensities are larger than those for He, because H_2 molecules explore a more corrugated PES. Though evaluation of realistic PESs for H_2/metal surface systems is not trivial and 6D quantum dynamical (QD) calculations are computationally demanding, an exact theoretical description of H_2 scattering from first principles (within the rigid surface model) is now possible [4, 5]. This possibility has renewed interest in H_2 diffraction from the experimental side and as a consequence, we have gained considerable insight into the H_2 dissociation dynamics at metal surfaces.

In this work we summarize H_2 diffraction studies performed in recent years. The main conclusions are the following:

(i) the diffraction patterns cannot be understood from differences in surface corrugation along different symmetry directions;
(ii) out-of-plane diffraction is important, and its importance increases with increasing reactivity;
(iii) the predictions of state-of-the-art 6D QD calculations within the Born–Oppenheimer approximation are corroborated by experiment and
(iv) classical dynamics calculations using a DFT determined 6D PES can be used to predict semi-quantitatively several experiments.

The diffraction of H_2 and D_2 molecular beams from surfaces is in principle very similar to He diffraction, the two major differences being (i) the possibility of rotational-state transitions in the case of molecular scattering and (ii) the fact that diffraction competes with the reactivity channel. Concerning (i), rotationally inelastic diffraction (RID) peaks can be observed in the form of additional diffraction peaks in the angular distributions. In this process, the incident molecules convert part of their translational energy into excitation of a rotational quantum level when colliding with the surface. The position of RID peaks within an angular distribution can be obtained by combining the Bragg condition for surface diffraction with conservation of

energy [21]:

$$\begin{aligned} \Delta\vec{K} &= \vec{K}_{\mathrm{f}} - \vec{K}_{\mathrm{i}} = \vec{G} \\ E_{\mathrm{f}} - E_{\mathrm{i}} &= \Delta E_{\mathrm{rot}}. \end{aligned} \tag{1.1}$$

In (1.1), $\vec{K}_{\mathrm{f}}$ and $\vec{K}_{\mathrm{i}}$ are the parallel components of the outgoing and incident wavevectors, respectively, $\vec{G}$ is a surface reciprocal lattice vector, E_{f} and E_{i} are the final and incident beam energies and ΔE_{rot} is the rotational transition energy. For H_2 (D_2) this energy is $|\Delta E_{\mathrm{rot}}| = 44.6$ (22.2) meV for the lowest transitions ($0 \rightarrow 2$ and $2 \rightarrow 0$) and $|\Delta E_{\mathrm{rot}}| = 74.3$ (36.88) meV for the $1 \rightarrow 3$ and $3 \rightarrow 1$ transitions.

As to the reactivity channel, a quantitative measure is given by the sticking probability S of H_2. This probability might vary from zero (for non-reactive systems, like noble metals) to a value very close to unity for highly reactive (also called non-activated) systems, like transition metal surfaces. As a consequence, on most reactive surfaces a hydrogen overlayer can build up quickly if the experiments are done at a surface temperature below the desorption temperature of H_2 ($\sim$350 K) and alter the measurements. This sets an important boundary condition to the experiments, which must be carried out at high surface temperatures, increasing the inelastic background.

2. Experimental set-ups

H_2 diffraction experiments from reactive surfaces are very demanding, because they require a high sensitivity (to detect reflectivities that are of the order of a few per cent [22]) combined with the possibility of recording both in-plane and out-of-plane spectra, since pronounced out-of-plane scattering occurs for these systems [22]. For this reason, the experiments reviewed in this work were carried out using two different apparatuses recently installed at the Universidad Autónoma de Madrid. A schematic representation of the two set-ups is shown in figure 1. In the first one, the detector can be rotated through 200° in the scattering plane (defined by the incident beam direction and the normal to the surface) as well as $\pm 15°$ from the scattering plane for a fixed angle of incidence. Another advantage of this set-up is that it allows measurement of the direct incident beam intensity, making possible very accurate determination of absolute diffraction probabilities. On the other hand, since the detector lies very close to the sample, the angular resolution is lower than for time-of-flight (TOF) systems, and the dynamical range is limited to $\sim 3 \times 10^{-3}$ of the incoming beam intensity.

The second apparatus is a high-resolution time-of-flight (TOF) spectrometer with a fixed angle of 106.8° between incident and outgoing beams. Angular distributions are measured by rotating the crystal about an axis normal to the plane of the incident and outgoing beams. After scattering through a fixed angle of $\theta_{\mathrm{SD}} = 106.8°$ with respect to the incident beam, the particles are detected by a home-made magnetic mass spectrometer detector located at 1.6985 m from the target surface. This allows detection of diffraction intensities as low as $\sim 10^{-4}$ of the incoming beam, while the angular resolution is determined by the detector acceptance angle, which is about 0.2°. Scattering experiments were carried out at energies between about 20 and 150 meV.

The rotational populations of the incident H_2/D_2 beams in our experiment were estimated from previous theoretical and experimental work [23]. For an incident energy $E_{\mathrm{i}} = 150$ meV, most H_2 molecules are in the $J_{\mathrm{i}} = 1$ state (60%) while 38% of D_2 molecules are in the $J_{\mathrm{i}} = 2$, 18% in the $J_{\mathrm{i}} = 1$ and 16% in the $J_{\mathrm{i}} = 0$ state. Because of the large spacing between the vibrational levels of the H_2 molecule, more than 99% of the molecules are in the $v_{\mathrm{i}} = 0$ state for $E_{\mathrm{i}} \leqslant 200$ meV.

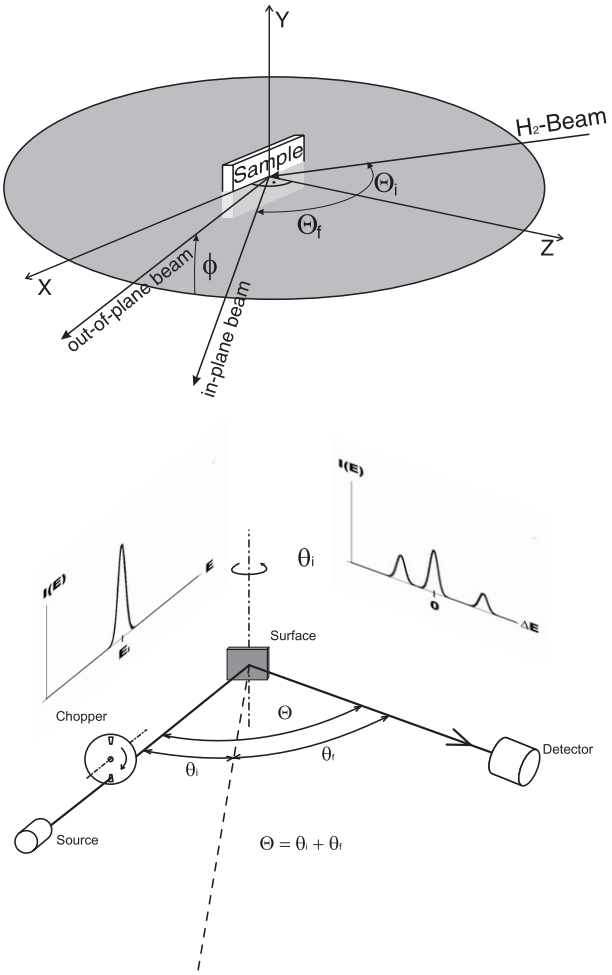

Figure 1. Molecular beam scattering apparatus recently installed at the Universidad Autónoma de Madrid. In the time-of-flight set-up (bottom), the angle of incidence is changed during a measurement by rotating the sample. In the one shown at the top, in contrast, the detector can be rotated in and out of the scattering plane while keeping the angle of incidence fixed.

The single-crystal surfaces employed in the experiments were cleaned *in situ* in UHV by ion sputtering and annealing. Details on Pd(111) [22], NiAl(110) [24, 25], Pt(111) [26] and Pd(110) [27] sample preparation can be found elsewhere. A scheme of the corresponding direct and reciprocal lattices of these surfaces is shown in figure 2.

3. Theoretical methods

In current theoretical approaches, the scattering dynamics of H_2 on metal surfaces is described in terms of a single six-dimensional molecule–surface PES obtained from state-of-the-art electronic structure calculations [4, 5]. This means that any excitation (electronic or phononic) of the surface is discarded. Inclusion of such inelastic effects in a quantum calculation modelling all six degrees of freedom of H_2 is at present unfeasible. In the context of

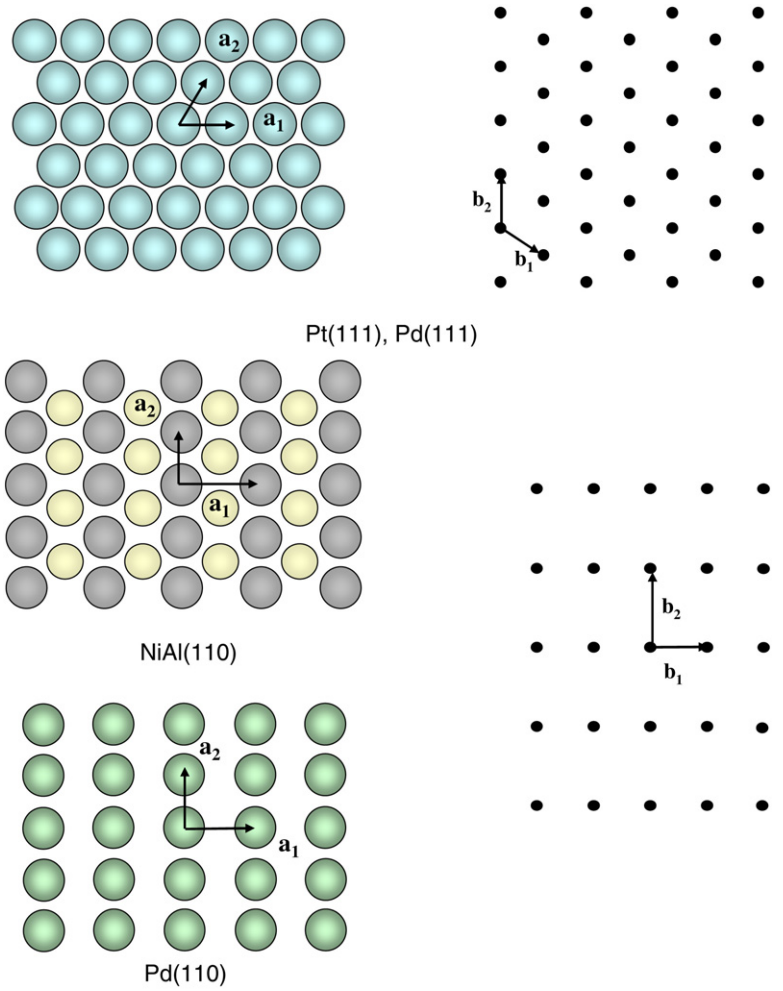

Figure 2. Top view of the direct and reciprocal lattices of Pt(111), Pd(111), NiAl(110), and Pd(110) indicating the basis vectors.

classical calculations, a few partial solutions have been proposed to include phonon inelastic processes (see, e.g., [28–30]). In the case of diffraction, increased surface temperature leads to smaller diffraction intensities, as observed experimentally, but maintaining the relative importance of the diffraction intensities. Thus, for the sake of consistency between different dynamical calculations, inelastic phonon effects have been neglected in all reported dynamical calculations. The approximation of neglecting electron–hole pair excitations can be justified on the basis of recent experimental results [26].

The methods used to describe the dynamics of the H_2–surface interaction were described in detail earlier. In particular, the PES of H_2/Pd(111) [31], H_2/Pt(111) [32], H_2/NiAl(110) [33], and H_2/Pd(110) [34] have been determined by interpolation of *ab initio* DFT/GGA data (GGA stands for generalized gradient approximation) using the corrugation reducing procedure (CRP) [35]. The CRP has been shown to provide a precision better than 30 meV in the dynamically relevant regions for several H_2–metal systems [31, 33, 32].

The above PESs have been used to perform 6D classical trajectory and quantum dynamics (QD) calculations. In the classical trajectory calculations one has to integrate the Hamilton equations using, in our case, the predictor–corrector method of Burlish and Stoer. Typically, the total energy for each trajectory is conserved to within 0.1 meV. To calculate dissociative adsorption probabilities, one has to compute between 5000 and 10 000 trajectories, but for state-to-state scattering probabilities (which are in general small) these numbers oscillate between 1×10^5 and 2×10^5 trajectories per incidence angle. The estimated statistical error of the probabilities is of the order of 1% for dissociative adsorption and 2% for reflection channels. In classical dynamics calculations the initial vibrational zero point energy (ZPE) of impinging molecules must be considered with caution. In so-called *quasi-classical* (QC) calculations, one makes use of a microcanonical distribution for the molecular vibrational motion with energy (ZPE) equal to that of the quantum ground state. Such calculations produce an artificial quenching of dynamic trapping [31]. On the other hand, the so-called *classical* (C) calculations, which disregard the initial ZPE, give low (high) adsorption (reflection) probabilities because the effect of vibrational softening, which accelerates the molecules towards the surface, is not accounted for [31]. Thus, in general, C sticking probabilities are lower than the QC ones. However, both QC and C calculations give very similar angular and rotational state distributions of scattered molecules. Another possibility is to run C calculations but adding to the PES an attractive term that accounts for the adiabatic vibration-to-translation energy transfer that takes place when the molecules approach the surface (CZPE calculations).

In either classical approach, the probability of a given (n, m) diffraction peak is evaluated as the fraction of trajectories in which the molecule scatters non-reactively with a parallel momentum change contained in the 2D Wigner–Seitz cell built around the (n, m) lattice point in reciprocal space [36]. This method has been shown to provide diffraction peak intensities in reasonable agreement with experiments and quantum dynamics calculations [22, 37, 36]. We will further elaborate upon this method in section 4.4.

The quantum dynamics calculations presented in this paper have been carried out using the time-dependent wavepacket (TDWP) method [38]. A direct discrete variable representation (DVR) [39] is used to represent the dependence of the wavefunction on X, Y, Z and r. Fast Fourier transformations are used to transform the wavefunction from the DVR to a direct product finite basis representation (FBR) in momentum space, and vice versa. A non-direct product FBR is used for the rotations, employing Gauss–Legendre and Fourier transformations to switch between the DVR and FBR [40, 41]. The initial wavefunction is the product of a Gaussian wavepacket in Z, a plane wave for the motion parallel to the surface and a rovibrational wavefunction describing the (v, J_i, m_{J_i}) initial state of H_2. The wavefunction, placed initially far from the surface, where the interaction with the surface is negligible, is propagated in time using the split-operator method [42], in which the kinetic and potential propagation part of the Hamiltonian are symmetrically split according to [43]:

$$\begin{aligned}\exp(-\mathrm{i}\hat{H}\Delta t) = {} & \exp(-\mathrm{i}\hat{K}\Delta t/2) \times \exp(-\mathrm{i}\hat{H}_{\mathrm{rot}}\Delta t/2) \times \exp(-\mathrm{i}\hat{V}\Delta t) \\ & \times \exp(-\mathrm{i}\hat{H}_{\mathrm{rot}}\Delta t/2) \times \exp(-\mathrm{i}\hat{K}\Delta t/2). \end{aligned} \tag{3.1}$$

Here, $\hat{V}$ is the potential describing the interaction of the H_2 molecule with the surface (as described by the PES), $\hat{H}_{\mathrm{rot}}$ is the kinetic energy operator associated with H_2 rotation, and $\hat{K}$ is the kinetic energy operator associated with the centre-of-mass motion of H_2 and the H–H relative motion. Finally, Δt is the time-step used in the split-operator formalism. Optical potentials are used to absorb the part of the wavepacket that has reacted and that has been reflected. The reflected wavepacket is analysed using a scattering amplitude formalism [44].

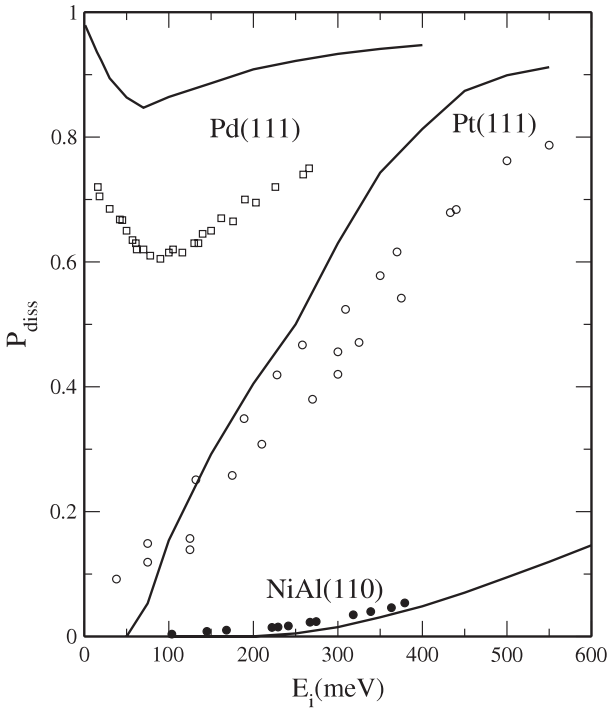

Figure 3. Experimental (symbols) and classical calculations (solid lines) of the sticking probability as a function of incident beam energy for NiAl(110), Pt(111) and Pd(111). See the text for details.

4. Results

4.1. Reactivity of NiAl(110), Pt(111) and Pd(111)

Figure 3 shows the dissociative sticking probability of H_2 on NiAl(110), Pt(111) and Pd(111) as a function of incident beam energy. Symbols correspond to supersonic molecular beam experiments [45–47] and the lines are the results of classical trajectory calculations [33, 48, 49]. For the three surfaces considered, classical results reproduce well the experimental trends. This strongly supports the use of the present theoretical approach (i.e. the Born–Oppenheimer approximation + DFT/GGA + classical molecular dynamics) to investigate adsorption mechanisms and their connection with experiments.

Figure 3 clearly shows an increasing reactivity when going from NiAl(110) to Pt(111) and Pd(111). On NiAl(110) and Pt(111), dissociative adsorption is an activated process, whereas it is non-activated on Pd(111). For H_2/NiAl(110) and H_2/Pt(111), the minimum activation barrier (obtained in DFT calculations) is ∼300 and ∼50 meV, respectively. These values determine the dissociation energy thresholds found in the classical results shown in figure 3 for these systems. An important difference between Pd(111) on the one hand, and Pt(111) and NiAl(110) on the other, is that, in the latter cases, the probability increases monotonically with E_i. Classical calculations show that on Pt(111) and NiAl(110) a single *direct* mechanism dominates adsorption. Thus, molecules approach the surface and directly dissociate or are scattered back to the vacuum after a single rebound on the surface [33]. For H_2/Pd(111) such a direct dissociation mechanism only dominates for energies above 100 meV. At low energies, an *indirect* mechanism usually called *dynamic trapping* also plays an important role [34, 49]. In this case, many molecules remain *trapped* during a long time due to energy exchange from perpendicular motion to rotation and parallel motion which prevents the molecules from

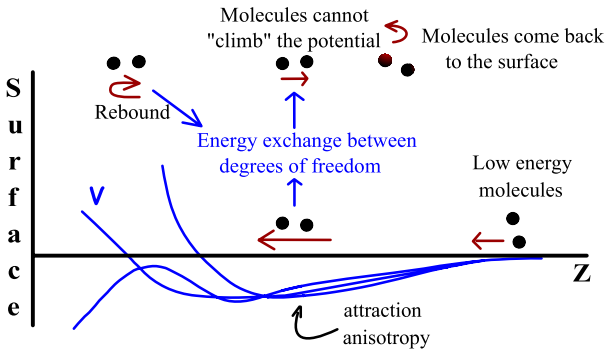

Figure 4. Dynamic trapping mechanism.

escaping the surface attraction (see figure 4). As a consequence, dynamic trapping enhances dissociative adsorption, but its role decreases when E_i increases. This produces the initial decrease of the sticking probability as a function of E_i observed for H_2/Pd(111). This subject will be discussed in more detail in section 4.5.

4.2. Molecular hydrogen diffraction experiments

Figure 5 shows experimental diffraction spectra obtained with (a) NiAl(110), (b) Pt(111), and (c) Pd(111). In the case of NiAl(110), the experimental data correspond to D_2 molecules impinging the surface along the $[1\bar{1}0]$ azimuth with $E_i = 100$ meV and angle of incidence $\theta_i = 32.8°$. The results for Pt(111) and Pd(111) correspond to H_2 molecules impinging the surfaces along the $[10\bar{1}]$ azimuth with $E_i = 121$ meV and $\theta_i = 43.7°$ and $E_i = 105$ meV and $\theta_i = 63.3°$, respectively. In all cases, both in-plane and out-of-plane diffraction spectra are presented. For the impact energies considered in figure 5 (all around $E_i \sim 110$ meV), it is clear that the total reflectivities of the three surfaces are quite different: i.e. going from ∼1 for NiAl(110) to ∼0.3 for Pd(111) (see experimental data of figure 3).

For NiAl(110), both first order in-plane and out-of-plane diffraction peaks are observed as well as RID peaks corresponding to the $0 \rightarrow 2$ and $2 \rightarrow 0$ transitions. In this case, out-of-plane peaks are less important than in-plane ones. Pt(111) has a relatively low reactivity, which is halfway between those of Pd(111) and NiAl(110). Accordingly, a large reflectivity is observed in experiments, as can be seen in the spectra presented in figure 5. For these incidence conditions, in-plane peaks are not observed, whereas out-of-plane ones are clearly resolved. For other incidence conditions, small in-plane peaks were observed, but still the general trend is that out-of-plane diffraction is more important than in plane. The large increase of the sticking probability when going from NiAl(110) and Pt(111) to Pd(111) entails a large decrease of the elastic reflectivity (up to ∼0.5%), and in particular of the specular peak. A remarkable feature of the Pd(111) spectrum is the appearance of pronounced out-of-plane diffraction, while no diffraction peaks are observed in the scattering plane [37]. Indeed, the intensity of the (01) peak is almost 45% of the specular one at $E_i = 150$ meV (shown in figure 7 below). These results show that out-of-plane diffraction is more important than previously assumed in H_2 diffraction experiments [2]. For instance, in view of the small intensity of in-plane diffraction peaks, it was first assumed that the corrugation of the HD/Pt(111) PES was small [50]. However, it was also observed later that the sticking probability of H_2 on Pt(111) does not satisfy normal energy scaling, which indicates a relatively large corrugation [46]. These contradictory conclusions were conciliated in the light of these results, which show that small in-plane diffraction peaks cannot be considered a definite proof of small corrugation and put in evidence the need for also measuring out-of-plane diffraction to assess the corrugation of the molecule–surface interaction

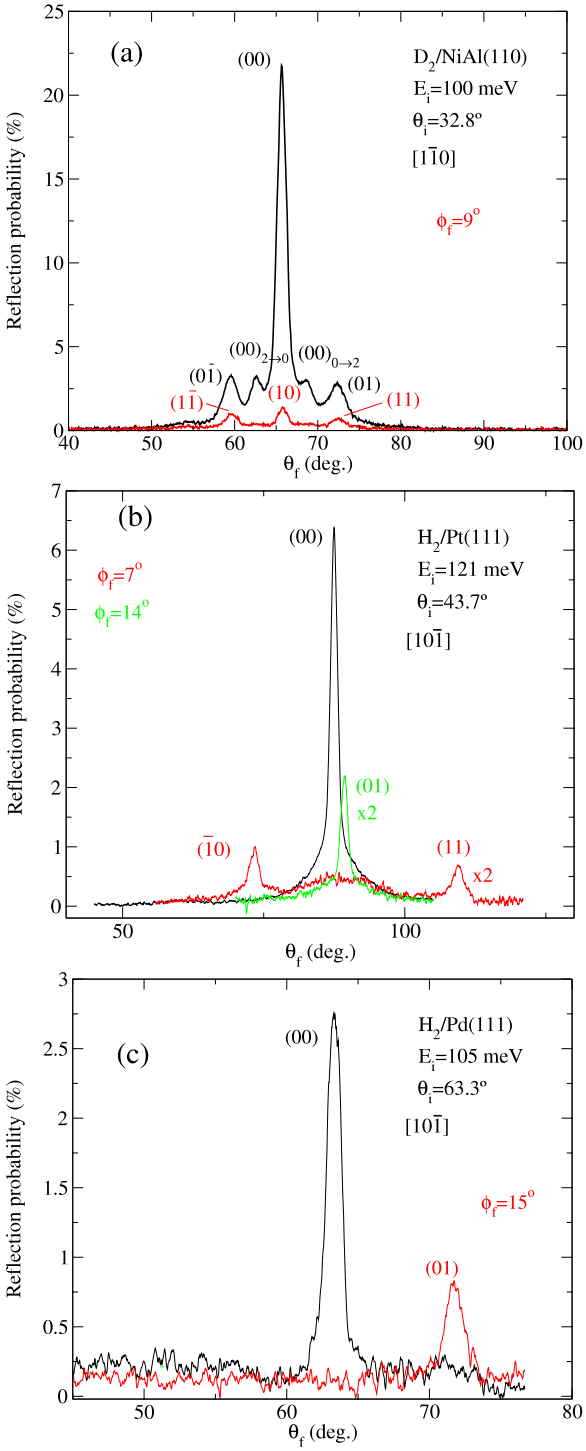

Figure 5. In-plane ($\phi_f = 0°$, black curves) and out-of-plane (red and green curves) H_2 diffraction spectra for NiAl(110), Pt(111) and Pd(111).

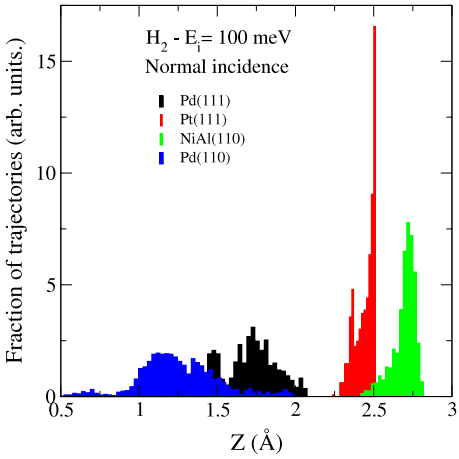

Figure 6. Closest approach distance for H_2 molecules scattered from NiAl(110), Pt(111), Pd(111) and Pd(110), for $E_i = 100$ meV and normal incidence.

potential (see [51] and references therein). Finally, it is interesting to note that the results presented in figure 5 suggest that the relative importance of out-of-plane diffraction increases when the reactivity of the surface increases.

Figure 6 shows the distribution of the closest approach distance to the surface of H_2 molecules scattered from NiAl(110), Pt(111), Pd(111) and Pd(110). The results correspond to $E_i = 100$ meV and normal incidence, and were obtained with classical trajectory calculations. The consequences of the different reactivities of the three surfaces on the scattering dynamics are clear. For H_2/NiAl(110), i.e. the less reactive system, the molecules are reflected far from the surface, between $Z = 2.5$ and 2.8 Å. The corresponding PES presents a repulsive behaviour in the entrance channel, and molecules impinging the surface with a perpendicular energy of 100 meV find a slightly corrugated hard-wall-like potential in that region [52]. As a consequence, specular reflection is dominant on this surface, and diffraction is relatively small.

For H_2/Pt(111), the closest approach distance of reflected molecules is smaller than in the case of NiAl(110) (between 2.25 and 2.5 Å) and is slightly larger than $Z_b \sim 2.1$ Å, which corresponds to the minimum activation barrier for dissociation of ∼50 meV [32, 53]. Then, it is expected that molecules reflected closer to the surface explore a more corrugated region of the PES, and accordingly diffraction peaks become more important compared to the specular one. This is consistent with the experimental data shown in figure 5. This effect is even clearer in the case of Pd surfaces. For instance, for H_2/Pd(111), molecules are reflected between ∼1.5 and 2 Å, where the PES corrugation is very strong. Accordingly, there is a strong suppression of the specular channel and, therefore, diffraction becomes relatively more important.

The relative amount of in-plane and out-of-plane diffraction depends on impact energy and incidence angle. This is the consequence of a dynamical effect associated with grazing incidence and not of a purely *static* one such as surface corrugation. A model has been proposed [54], based on the periodicity of the potential along the incidence direction. Such periodicity implies that, along the incidence direction, any increase (decrease) of the molecule linear momentum is compensated by a decrease (increase), while the variation of the transverse linear momentum is cumulative [54]. The model suggests that this effect should also be expected in the scattering of light atoms if they approach close enough to the surface. Since out-of-plane diffraction dominates for large incidence angles, it is not surprising that the (01) peak is comparable to the specular one in the H_2/Pd(111) system. Our classical dynamics calculations show a similar suppression of the specular peak in D_2/NiAl(110) at high impact energies.

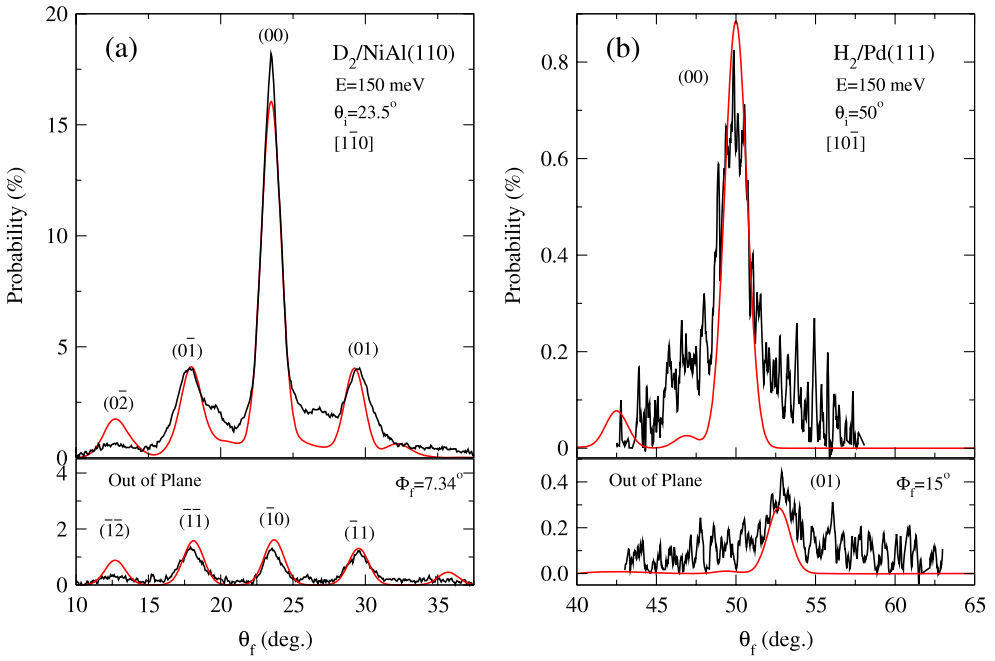

Figure 7. In-plane and out-of-plane H_2 diffraction spectra for NiAl(110) (left) and Pd(111) (right). Black curves, experiment; red lines, 6D quantum dynamical calculation. Theoretical calculations have been convoluted with a Gaussian function of width $\sigma = 0.7°$ to account for the limited angular resolution of the measurements. Both the experimental results and the calculations have been normalized to the height of the specular peak that arises from the quantum calculations.

4.3. Comparison with 6D quantum calculations

Figure 7 shows a comparison between experiment and 6D quantum calculations for both Pd(111) and NiAl(110) surfaces. Figure 8 shows similar results obtained for Pt(111) and several incident beam energies. In this case, the comparison was made after extrapolating the experimental data measured at 463 to 0 K according to the Debye–Waller model, i.e. it corresponds to *absolute* diffraction probabilities [26].

The good agreement obtained for all systems suggests that quantum dynamics calculations treating all molecular degrees of freedom can accurately predict diffraction patterns for hydrogen scattering from reactive metal surfaces. Inclusion of all molecular degrees of freedom is essential to account for the competition between dissociative and non-dissociative channels. This supports the use of 6D DFT theories to properly describe the H_2–surface interaction even in regions far away from the surface. Finally, it shows that out-of-plane diffraction measurements are crucial to test the details of the PES in a wide region of space.

4.4. Classical diffraction

It may well come as a surprise to many that classical mechanics can be used to predict intensities for molecular diffraction, which has always been viewed as a typical quantum phenomenon. Indeed, diffraction was used in the 1920s to prove the wave nature of atomic and molecular motion. According to Bragg's law, diffraction is observed when the variation of the linear momentum parallel to the surface is restricted to well defined discrete values. In contrast, linear momentum changes continuously in a classical world. Discretization methods that make

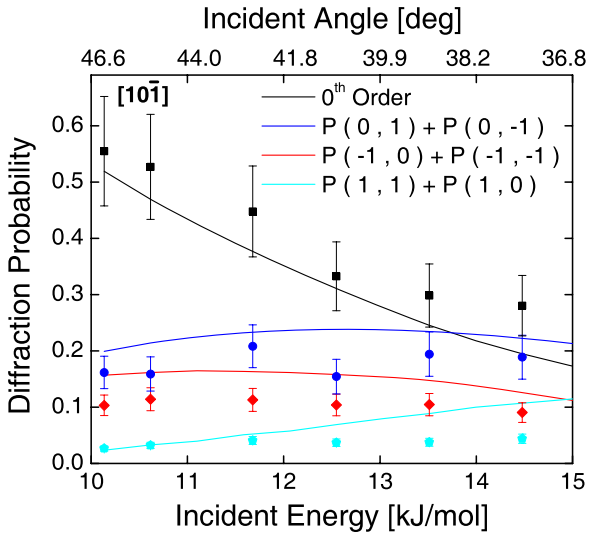

Figure 8. Experimentally determined H_2 diffraction probabilities (symbols) are compared with computed diffraction probabilities (curves), for specular scattering (black colour) and several first order out-of-plane (purple and red colour) and in-plane (light blue and pink colour) diffractive scattering transitions. The results are for incidence along the [10$\bar{1}$] direction. Probabilities for symmetry equivalent transitions were summed. Error bars represent 68% confidence intervals. From [26].

classical trajectory calculations compatible with Bragg's law were first proposed by Ray and Bowman in 1975 [55, 56].

One has to look for a procedure that is compatible with Bragg's law, i.e. that leads to a $\mathbf{k}$ histogram that allows one to assign a classical trajectory with final momentum $\mathbf{p}_f$ to one of the diffraction peaks. From Bragg's law, the variation of parallel momentum, $\hbar\Delta\mathbf{K}^{\parallel} = \hbar(\mathbf{K}_f^{\parallel} - \mathbf{K}_i^{\parallel})$, must coincide with one of the vectors of the reciprocal lattice (up to $\hbar$). Since there is not such a restriction in classical calculations, $\Delta\mathbf{P}^{\parallel}$ can be any vector in the plane that defines the surface in reciprocal space. We divide this plane into identical regions, such that each region corresponds to the Wigner–Seitz cell around each lattice point in reciprocal space. Thus, each cell is unambiguously associated with a lattice vector and, therefore, with a diffraction peak. Then, one can easily assign all classical trajectories with a value of $\Delta\mathbf{P}^{\parallel}$ contained in a given Wigner–Seitz cell to the corresponding (n, m) vector of the reciprocal lattice. The diffraction probability $P_{n,m}$ is given by the number of trajectories $N_{n,m}$ in which the molecule scatters non-reactively with $\Delta\mathbf{P}^{\parallel}$ in the (n, m) Wigner–Seitz cell divided by the total number of trajectories N_{tot}:

$$P_{n,m} = N_{n,m}/N_{\text{tot}}. \tag{4.1}$$

The calculated probabilities are assumed to be proportional to the diffraction intensities observed experimentally.

In figure 9 we compare the results of this method with those obtained from quantum dynamical calculations using the same PES. Our benchmark is the H_2/Pd(111) system. The left panel corresponds to normal incidence, $E_i = 200$ meV and $J_i = 0$. This is the simplest case because, for normal incidence, all directions associated with first order diffraction peaks are equivalent (or nearly equivalent for higher diffraction orders) and, therefore, the corresponding peaks have the same intensity. It can be seen that classical results are close to the quantum

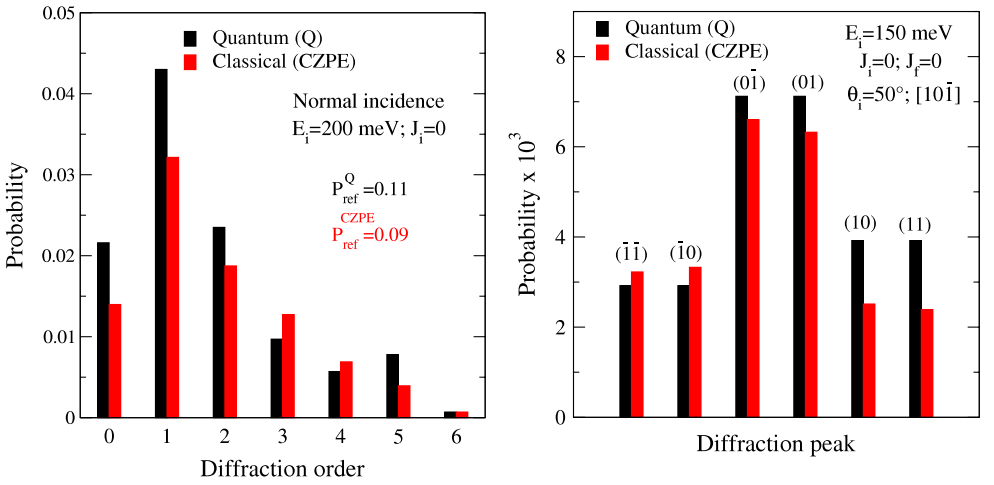

Figure 9. Probabilities of diffraction orders for H_2/Pd(111). Left: normal incidence. Right: incidence angle of 50°. Black columns: results of quantum calculations. Red columns: results of the classical diffraction method applied to classical calculations that include the ZPE.

ones for all diffraction orders. The results shown on the right panel correspond to an angle of incidence of 50°, $E_i = 150$ meV and $J_i = 0$. Again, a remarkably good agreement is obtained. This indicates that the molecule–surface dynamics leading to diffraction is to a large extent classical in nature.

4.5. Pd(110): evidence of dynamic trapping

In this section we will discuss the results on Pd(110), which is an excellent example of a system where diffraction data are essential to understand the H_2 scattering dynamics. In effect, the data presented in figure 10 show that the sticking coefficient of H_2 is comparable on the two surfaces. However, the corresponding diffraction spectra look very different. Figure 11 shows an in-plane H_2-diffraction spectrum recorded along the [001] azimuth of Pd(110) (red curve). The comparison with a typical H_2-diffraction spectrum in Pd(111) (shown in figure 5(c)) is surprising: whereas intense specular reflection is observed from Pd(111), diffraction is completely suppressed from Pd(110). The same behaviour was observed at different incident energies between 25 and 150 meV and angles of incidence (measured from the surface normal) from 40° to 70°. In all cases, out-of-plane spectra were also measured, since it is known that this channel is important for H_2 diffraction. No evidence for H_2 diffraction from Pd(110) was found. Similar results have been obtained along the [10$\bar{1}$] azimuth. Notice that the absence of H_2 diffraction peaks in Pd(110) cannot be attributed to inelastic processes, since H_2 diffraction is clearly observed from Pd(111) at the same surface temperature, $T_s = 435$ K.

To exclude a poor quality Pd(110) surface as the possible origin of this behaviour, an in-plane HAS spectrum is shown in the same panel. The existence of several diffraction peaks proves that we are dealing with a clean, well ordered Pd(110) surface. These results are very surprising and demonstrate that H_2 reflected peak intensities from Pd(110) are below 3×10^{-3} of the incoming beam intensity. To have access to even weaker intensities, we have performed the same experiment with the high-sensitivity TOF machine described in section 2. The results are presented in figure 12(a). Again, pronounced He diffraction is observed (even third order peaks), but there is no trace of reflected peaks with D_2. Notice, however, that now the difference

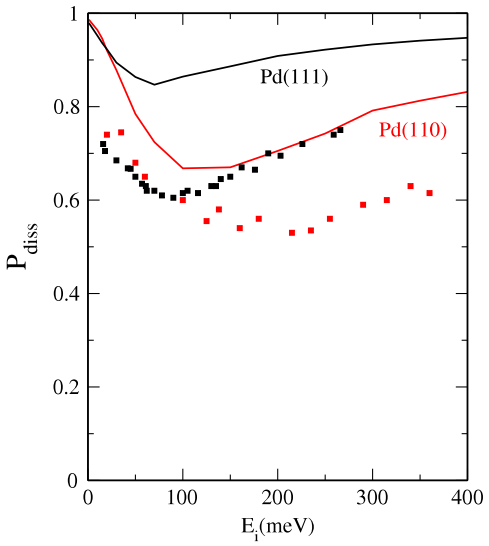

Figure 10. Sticking coefficient of H_2 on Pd(111) and Pd(110). Solid lines: classical calculations [34]. Symbols: experiment [47, 57].

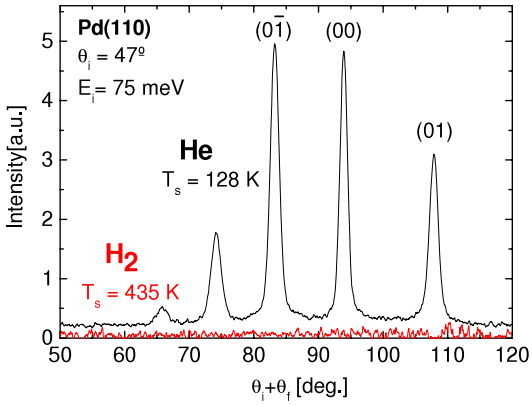

Figure 11. In-plane H_2 (red curve) and He (black curve, shifted upwards for clarity) angular distributions recorded from Pd(110). The incidence direction is along the $[10\bar{1}]$ azimuth for Pd(111), and along [001] for Pd(110).

in intensity between the He specular peak and the D_2 background is almost three orders of magnitude. Therefore, reflected peaks, if they exist, must have intensities below 10^{-4} of the incoming D_2 beam intensity. It is worth emphasizing that, using a TOF machine similar to ours, pronounced specular and first-order D_2 diffraction was observed along the same azimuth from Rh(110) at $T_s \sim 400$ K [58] and Ni(110) at $T_s \sim 700$ K [59], which exhibit an even lower reflectivity ($S_0 \sim 0.9$ [60]) than Pd(110).

In order to check that the beam alignment was not affected by changing from He to D_2, we have recorded an additional spectrum by cooling down the sample to 130 K in the same run. At this temperature, the Pd(110) surface is saturated by atomic hydrogen, forming a (2×1)H structure, and becomes much less reactive [61]. Figure 12(b) shows that, under these conditions, diffraction peaks are clearly observed, in particular the specular one. Of course, this spectrum tells us nothing about the reflection mechanisms on clean Pd(110), but proves that the corresponding D_2 experiment at 430 K is meaningful.

To understand the origin of these observations, we have carried out classical trajectory calculations [62] using the same initial conditions as in the present experiments. We have used the *ab initio* six-dimensional H_2/Pd(110) PES reported in [34] for a rigid surface.

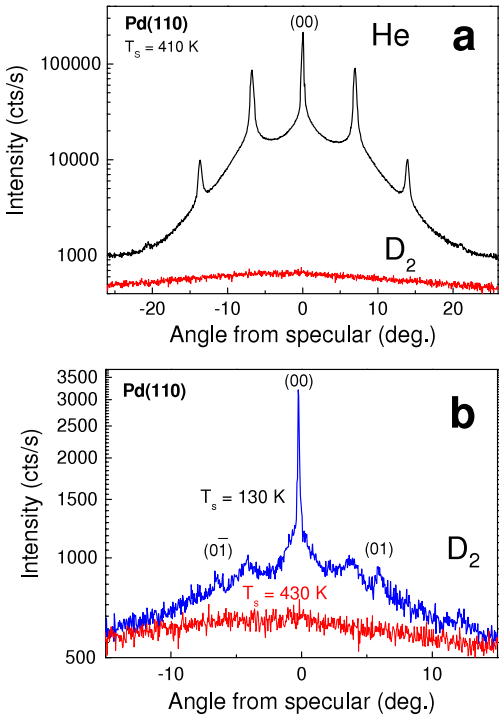

Figure 12. (a) Angular distributions of He (black curve) and D_2 (red curve) scattered from Pd(110) at $T_s = 430$ K, measured with the TOF apparatus. The incidence direction is along [001]. (b) Comparison of the D_2 spectrum taken at $T_s = 430$ K with the one measured after cooling down the sample to $T_s = 110$ K with the D_2 beam on (blue curve).

A relatively small difference in reactivity like the one found between H_2/Pd(111) and H_2/Pd(110) can still entail different behaviours of scattered molecules. In figure 13(a), we show the ratio of scattered molecules that have been temporarily trapped and the total number of unreactive scattered molecules as a function of E_i (for normal incidence and $H_2(v = 0, J = 0)$). For Pd(110), at low energies a large fraction of scattered molecules have been trapped, whereas on Pd(111) scattering is essentially direct. However, this does not mean that trapping does not take place on Pd(111). Both surfaces attract H_2 molecules in the entrance channel (i.e. above ∼2 Å) and the variation of the PES with molecular orientation and position on the unit cell produces energy exchange between degrees of freedom that results in molecules becoming trapped. However, the larger number of energetically (and dynamically) accessible dissociation pathways means that on Pd(111) almost all trapped molecules dissociate, whereas on Pd(110) trapped molecules still have a non-negligible probability to be scattered back to vacuum, as shown schematically in figure 14. This results in very different angular distributions of molecules scattered from Pd(111) and Pd(110) at low energies (figure 13(b)). For H_2/Pd(110) a cosine-like distribution is observed as a consequence of the memory loss of a large fraction of scattered molecules, whereas for H_2/Pd(111) the essentially direct scattering mechanism leads to the appearance of a pronounced peak of reflected molecules in the specular direction ($\theta_f = \theta_i$) [62, 63].

The absence of the specular peak for H_2 and D_2 diffraction from Pd(110) is reminiscent of the selective adsorption resonance processes well known in the case of HAS (see [64] and references therein). In the present case, the attraction felt by H_2 molecules in the entrance

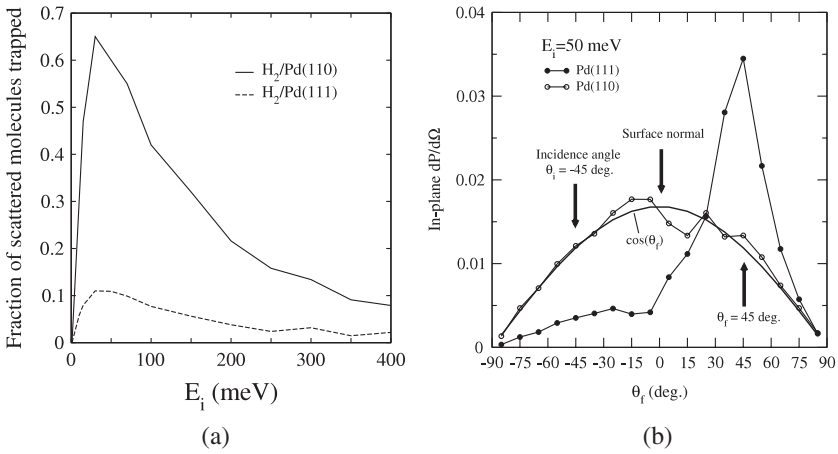

Figure 13. Classical trajectory calculations for H_2/Pd(111) and H_2/Pd(110). (a) Fraction of reflected molecules after trapping as a function of E_i (at normal incidence) for H_2/Pd(111) and H_2/Pd(110). (b) Angular distribution of scattered low energy H_2 molecules ($\theta_i = 45°$ and $E_i = 50$ meV).

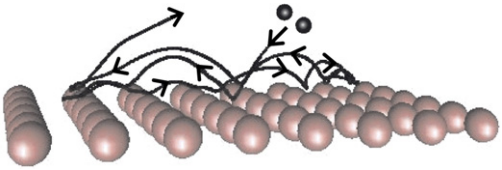

Figure 14. Typical trajectory followed by a first trapped and then reflected molecule.

channel is much stronger than in the case of He atoms interacting with metal surfaces (the well depth for H_2/Pd is about one order of magnitude larger than the physisorption well for He/metal surfaces [65, 66]). Thus, for H_2/Pd(110), dynamic trapping is possible and efficient for a wide range of initial impact conditions, preventing the observation of the specular diffraction peak in experiments.

5. Conclusion and perspectives

We have reviewed recent experimental work on diffraction of H_2 at metal surfaces in combination with theory. It has been shown that, with the help of state-of-the-art 6D quantum and classical dynamics calculations within the Born–Oppenheimer approximation, diffraction measurements can provide considerable insight into the H_2 dissociation dynamics at these surfaces. Contrary to earlier expectations, diffraction patterns cannot be understood only from differences in surface corrugation along different symmetry directions. Furthermore, out-of-plane diffraction is important, and its importance increases with increasing reactivity.

Measurements on NiAl(110) [25], Pt(111) [26], Ni(110) [59] and Cu(001) [67] have shown that the attenuation of the H_2 diffraction peaks intensity due to surface temperature is reasonably described by a simple Debye–Waller model. This explains the excellent agreement between theory and experiment for all the systems presented in this work even though thermal vibrations of surface atoms (phonons) were not included in the calculations.

In spite of this progress, there are still some open questions that deserve further investigations. A good example is provided by the rotationally inelastic diffraction (RID) peaks. In general, both classical and quantum dynamics calculations underestimate the intensity of

such diffraction peaks. This has been observed, e.g., in H_2/NiAl(110) [68]. Whether this is the consequence of describing rotational excitation within the rigid surface approximation or is due to limitations in diffraction experiments is not yet clear. In this respect, the use of high-resolution time-of-flight devices, which can unambiguously resolve RID peaks that overlap elastic diffraction peaks, may be useful to settle this issue.

Also in connection with RID, it has been theoretically suggested [69] that the substantial reduction in the reflection probability that is observed when the dissociative channel becomes dominant can lead to a substantial reduction of RID, which would be the result of 'parallel' molecules going into the dissociation channel. This is because molecular rotation favours dissociation, thus leading to a competition between dissociation and rotational excitation of reflected molecules above the dissociation threshold. Measurements on rotational excitation might thus bring indirect evidence on the dissociation dynamics. Since verification of this prediction requires the use of molecular beams with energy well above the thresholds for rotational excitation, the ideal systems are those with dissociation barriers of the order of 100 meV or larger.

Certainly one of the most challenging and interesting future developments could concern the study of the reactivity of more complex systems, like the surfaces of thin films or multicomponent alloys, with the aim of tailoring surfaces with well defined dissociation properties. Our results also suggest that theory can provide a better understanding of detailed processes involved in more fundamental questions, like the influence of steps, kinks and vacancies on the H_2 dissociation dynamics.

Acknowledgments

Work supported by the DGI (project No CTQ2004-00039/BQU), the Comunidad de Madrid (CAM contract S-0505-MAT-0194), the AECI projects Nos A/3067/05 and A/4722/06, the BSCH-UAM agency and the 'Programa Ramón y Cajal'. We thank the CCC–UAM for their generous allocation of computer time, as well as K H Rieder and J P Toennies for the donation of the scattering apparatus used in our experiments. We are grateful to our co-workers D Barredo, C Díaz, G J Kroes, G Laurent, P Nieto, P Rivière and A Salin for fruitful discussions.

References

[1] Rettner C T and Ashfold M N R (ed) 1991 *Dynamics of Gas–Surface Interactions* (London: Royal Society of Chemistry)
[2] Bertino M F and Farías D 2002 *J. Phys.: Condens. Matter* **14** 6037
[3] Darling G R and Holloway S 1995 *Rep. Prog. Phys.* **58** 1595
[4] Gross A 1998 *Surf. Sci. Rep.* **32** 291
[5] Kroes G J 1999 *Prog. Surf. Sci.* **60** 1
[6] Kroes G J, Gross A, Baerends E J, Scheffler M and McCormack D A 2002 *Acc. Chem. Res.* **35** 193
[7] Hayden B E and Lamont C L A 1989 *Phys. Rev. Lett.* **63** 1823
[8] Michelsen H A, Rettner C T and Auerbach D J 1992 *Phys. Rev. Lett.* **69** 2678
[9] Hou H, Gulding S J, Rettner C T, Wodtke A M and Auerbach D J 1997 *Science* **277** 80
[10] Hodgson A, Moryl J, Traversaro P and Zhao H 1992 *Nature* **356** 501
[11] Gostein M, Watts E and Sitz G O 1997 *Phys. Rev. Lett.* **79** 2891
[12] Traeger F and Toennies J P 2004 *J. Phys. Chem.* B **108** 14710
[13] Benedek G, Traeger F and Toennies J P 2005 *Phys. Rev. Lett.* **94** 086103
[14] Skofronick G J, Toennies J P, Traeger F and Weiss H 2003 *Phys. Rev.* B **67** 035413
[15] Bertino M F, Glebov A L, Toennies J P, Traeger F, Pijper E, Kroes G J and Mowrey R C 1998 *Phys. Rev. Lett.* **81** 5608
[16] Berndt R, Toennies J P and Woell Ch 1990 *J. Chem. Phys.* **92** 1468
[17] Hodgson A, Samson P, Wight A and Cottrell C 1997 *Phys. Rev. Lett.* **78** 963

[18] Farías D and Rieder K H 1998 *Rep. Prog. Phys.* **61** 1575
[19] Halstead D and Holloway S 1988 *J. Chem. Phys.* **88** 7197
[20] Holloway S and Darling G R 1994 *Surf. Rev. Lett.* **1** 115
[21] Mattera L, Musenich R, Salvo C and Terreni S 1985 *Faraday Discuss. Chem. Soc.* **80** 115–26
[22] Farías D, Díaz C, Rivière P, Busnengo H F, Nieto P, Somers M F, Kroes G J, Salin A and Martín F 2004 *Phys. Rev. Lett.* **93** 246104
[23] Faubel M, Gianturco F A, Ragnetti F, Rusin L Y, Sondermann F and Tappe U 1994 *J. Chem. Phys.* **101** 8800
Miller D R 1988 *Atomic and Molecular Beam Methods* vol 1, ed G Scoles (New York: Oxford University Press) pp 14–53
[24] Farías D, Patting M and Rieder K H 2002 *J. Chem. Phys.* **117** 1797
[25] Farías D, Miranda R and Rieder K H 2002 *J. Chem. Phys.* **117** 2255
[26] Nieto P, Pijper E, Barredo D, Laurent G, Olsen R A, Baerends E J, Kroes G J and Farías D 2006 *Science* **312** 86
[27] Barredo D, Laurent G, Díaz C, Nieto P, Busnengo H F, Salin A, Farías D and Martín F 2006 *J. Chem. Phys.* **125** 051101
[28] Wahnström G, Lee A B and Strömquist J 1996 *J. Chem. Phys.* **105** 326
[29] Busnengo H F, Dong W, Sautet P and Salin A 2001 *Phys. Rev. Lett.* **87** 127601
[30] Pineau N, Busnengo H F, Rayez J C and Salin A 2005 *J. Chem. Phys.* **122** 214705
[31] Busnengo H F, Crespos C, Dong W, Rayez J C and Salin A 2002 *J. Chem. Phys.* **116** 9005
[32] Olsen R, Busnengo H F, Salin A, Somers M F, Kroes G J and Baerends E J 2002 *J. Chem. Phys.* **116** 3841
[33] Rivière P, Busnengo H F and Martín F 2005 *J. Chem. Phys.* **123** 074705
[34] Di Césare M A, Busnengo H F, Dong W and Salin A 2003 *J. Chem. Phys.* **118** 11226
[35] Busnengo H F, Salin A and Dong W 2000 *J. Chem. Phys.* **112** 7641
[36] Díaz C, Busnengo H F, Rivière P, Farías D, Nieto P, Somers M F, Kroes G J, Salin A and Martín F 2005 *J. Chem. Phys.* **122** 154706
[37] Farías D, Díaz C, Nieto P, Salin A and Martín F 2004 *Chem. Phys. Lett.* **390** 250
[38] Kosloff R 1988 *J. Phys. Chem.* **92** 2087
[39] Light J C, Hamilton J P and Lill J V 1985 *J. Chem. Phys.* **82** 1400
[40] Corey G C and Lemoine D 1992 *J. Chem. Phys.* **97** 4115
[41] Lemoine D 1994 *J. Chem. Phys.* **101** 10526
[42] Feit M D, J A F Jr and Steiger A 1982 *J. Comput. Phys.* **47** 412
[43] Dai J and Light J C 1997 *J. Chem. Phys.* **107** 1676
[44] Mowrey R C and Kroes G J 1995 *J. Chem. Phys.* **103** 1216
[45] Beutl M, Rendulic K D and Castro G R 1995 *J. Chem. Soc. Faraday Trans.* **91** 3639
[46] Luntz A C, Brown J K and Williams M D 1990 *J. Chem. Phys.* **93** 5240
[47] Beutl M, Lesnik J, Rendulic K D, Hirschl R, Eichler A, Kresse G and Hafner J 2001 *Chem. Phys. Lett.* **342** 473
[48] Pijper E, Somers M F, Kroes G J, Olsen R A, Baerends E J, Busnengo H F, Salin A and Lemoine D 2001 *Chem. Phys. Lett.* **347** 277
[49] Busnengo H F, Crespos C, Dong W, Rayez J C and Salin A 2002 *J. Chem. Phys.* **116** 9005
[50] Cowin J P, Yu Ch F, Sibener S J and Wharton L 1983 *J. Chem. Phys.* **79** 3537
[51] Kingma S M *et al* 2003 *J. Chem. Phys.* **118** 4190
[52] Rivière P, Busnengo H F and Martín F 2004 *J. Chem. Phys.* **121** 751
[53] Olsen R A, Kroes G J and Baerends E J 1999 *J. Chem. Phys.* **111** 11155
[54] Farías D, Díaz C, Nieto P, Salin A and Martín F 2004 *Chem. Phys. Lett.* **390** 250
[55] Ray C J and Bowman J M 1975 *J. Chem. Phys.* **63** 5231
[56] Ray C J and Bowman J M 1977 *J. Chem. Phys.* **66** 1122
[57] Resch Ch, Berger H F, Rendulic K D and Bertel E 1994 *Surf. Sci.* **316** L1105
[58] Cvetko D, Morgante A, Santaniello A and Tommasini F 1996 *J. Chem. Phys.* **104** 7778–83
[59] Bertino M F, Hofmann F and Toennies J P 1997 *J. Chem. Phys.* **106** 4327
[60] Christmann K 1988 *Surf. Sci. Rep.* **9**
[61] Rieder K H, Baumberger M and Stocker W 1983 *Phys. Rev. Lett.* **51** 1799
[62] Díaz C, Martín F, Busnengo H F and Salin A 2004 *J. Chem. Phys.* **120** 321
[63] Díaz C, Busnengo H F, Martín F and Salin A 2003 *J. Chem. Phys.* **118** 2886
[64] Hoinkes H and Wilsch H 1992 *Helium Atom Scattering from Surfaces* (*Springer Series in Surface Sciences* vol 27) ed E Hulpke (Berlin: Springer) p 113
[65] Petersen M, Wilke S, Ruggerone P, Kohler B and Scheffler M 1996 *Phys. Rev. Lett.* **76** 995
[66] Jean N, Trioni M I, Brivio G P and Bortolani V 2004 *Phys. Rev. Lett.* **92** 013201
[67] Bertino M F, Graham A P, Rusin L Y and Toennies J P 1998 *J. Chem. Phys.* **109** 8036
[68] Rivière P, Somers M F, Kroes G J and Martín F 2006 *Phys. Rev.* B **73** 205417
[69] Rivière P, Salin A and Martín F 2006 *J. Chem. Phys.* **124** 084706